Available online at www.sciencedirect.com
ScienceDirect
Catalysis Today 118 (2006) 73–84
CATALYSIS TODAY
www.elsevier.com/locate/cattod

Description of the pervaporation dehydration performance of A-type zeolite membranes: A modeling approach based on the Maxwell–Stefan theory

Marc Pera-Titus, Joan Llorens *, Javier Tejero, Fidel Cunill

Chemical Engineering Department, University of Barcelona, 08028 Barcelona, Spain

Available online 14 July 2006

Abstract

The dehydration performance of zeolite NaA membranes was investigated for the pervaporation (PV) of ethanol/water mixtures. High quality zeolite NaA membranes were prepared onto the inner-side of α-alumina tubular supports by the secondary growth method with a cross-flow filtration seeding combined with further semi-continuous hydrothermal syntheses (two cycles). The PV performance of the as-synthesized membranes was explored at 303–363 K for water compositions 1–60 wt.% and for feed and permeate pressures in the range 0–7 bar (relative) and 2–70 mbar, respectively. The selectivity was found to show a maximum at a water feed composition in the range 5–10 wt.% and to rise with temperature. Water and ethanol fluxes were successfully fitted to an adsorption–solution model derived from the Maxwell–Stefan theory, where ethanol flux is coupled with water flux. The adsorption of water and ethanol on the feed/membrane interface appears to govern the PV performance of zeolite NaA membranes.

Keywords: Zeolite membrane; Zeolite NaA; Pervaporation; Alcohol dehydration; Adsorption; Diffusion; Modeling

1. Introduction

Pervaporation (PV) is a membrane separation process that has gained increasing interest on the part of the chemical industry as an effective and energy-efficient technology to carry out separations that are troublesome or difficult to achieve by conventional means (i.e. distillation, extraction or adsorption), such as azeotropic and close-boiling liquid mixture separation, organic solvent dehydration and recovery of high added-value dilute species from water [1,2]. The technique is termed ''pervaporation'' because it involves the permselective ''vaporization'' of a liquid mixture (feed) through a suitable membrane whose downstream pressure is usually kept under vacuum [2]. Since different species permeate through the membrane at very different rates, a substance at low concentration in the liquid feed can be highly enriched in the vapor permeate. Thus, separation occurs, the pervaporative efficiency being strongly determined by the physicochemical nature of the membrane and by the kind of feed mixture to be separated.

Polymeric membranes have been widely investigated for PV membrane-based solvent separations and for reactive separations (either alone or integrated into hybrid distillation or extraction processes) [1–6]. However, their practical use has been limited owing to the insufficiency of their thermal, mechanical and chemical stability [2]. In order to overcome these shortcomings and to improve the membrane multipurpose character, extensive research has been directed in the past decades towards the development of inorganic membranes with suitable PV performance [7].

Nevertheless, the potential of using inorganic microporous materials (e.g., amorphous silica [8,9] and zeolites [7,10]) for both industrial and laboratory-scale PV applications has only been realized in recent years. In particular, zeolite membranes (usually consisting of a polycrystalline zeolitic layer grown on porous flat or tubular supports) have attracted widespread attention, because they take advantage of the unique properties of zeolites (e.g., highly crystalline ordered structure, molecular-sized pores, thermal stability and resistance to harsh environments, to swelling and to microbiological attack) in a film-like

* Corresponding author. Tel.: +34 934021304; fax: +34 934021291.
E-mail address: llorensl@ub.edu (J. Llorens).

0920-5861/$ – see front matter © 2006 Elsevier B.V. All rights reserved.
doi:10.1016/j.cattod.2005.12.006

Nomenclature

a	Activity
A, B	Parameters in the Antoine Eq. for vapor saturation pressure (A [K^{-1}], B
A^s	Pre-exponential factor of MS surface diffusivity [$m^2\ s^{-1}$]
A^S_{eff}	Effective pre-exponential factor of MS surface diffusivity according to Eq. (17) [$m^2\ s^{-1}$]
D^s	Fickian surface diffusivity [$m^2\ s^{-1}$]
$Đ^S_{ij}$	Counter-exchange MS diffusivity between the adsorbed species i and j [$m^2\ s^{-1}$]
$Đ^S_{iV}$	MS surface diffusivity of the adsorbed species i [$m^2\ s^{-1}$]
$Đ^S_{iV}(0)$	MS surface diffusivity of the adsorbed species i at zero coverage [$m^2\ s^{-1}$]
E^s	Activation energy of the MS surface diffusivity [kJ mol^{-1}]
E^S_{eff}	Effective activation energy defined according to Eq. (16) [kJ mol^{-1}]
M	Molecular weight [kg mol^{-1}]
N^s	Surface flux [kg $m^{-2}\ s^{-1}$]
p	Partial pressure [Pa]
P^0	Saturation vapor pressure [Pa]
P_f	Feed (retentate) relative pressure [Pa]
P_v	Permeate vapor pressure [Pa]
q	Molar loading [mol kg^{-1}]
q_M	Molar saturation loading [mol kg^{-1}]
Q	Permeability [kg $m^{-1}\ h^{-1}$]
R	Gas constant [8.314 Pa m^3 mol^{-1} K^{-1}]
T	Temperature [K]
T_{ref}	Reference temperature (mean value of experimental temperatures) [K]
x	Molar fraction in the liquid feed
X	Weight fraction in the liquid feed
y	Molar fraction in the vapor permeate
Y	Weight fraction in the vapor permeate

Greek symbols

$\alpha_{W/E}$	Selectivity of the membrane towards the separation of water
ΔH^0	Enthalpy of adsorption [kJ mol^{-1}]
ΔS^0	Entropy of adsorption [J mol^{-1} K^{-1}]
γ	Activity coefficient
K^s	Adsorption constant [Pa^{-1}]
ℓ	Thickness of the zeolite layer [m]
μ	Chemical potential [J mol^{-1}]
ρ_s	Density of zeolite NaA [1900 kg m^{-3}]
θ	Surface coverage
Γ_{ij}	Thermodynamic factors between species i and j according to Eq. (2)
∇	Nabla operator [m^{-1}]

Subscripts/superscripts

E	Ethanol
L	Liquid feed (retentate) of the membrane module in the PV experiments
v	Vapor permeate of the membrane module in the PV experiments
V	Vacant sites
W	Water

configuration [7]. These attributes make zeolite membranes attractive alternatives for separating mixtures whose components display adsorption or size differences, but are difficult to perform using either polymeric membranes or other conventional separation techniques. Among the great number of zeolite membranes reported in the literature (more than 14 [10]), those containing high Al/Si ratios (i.e. zeolite NaA [11–16], mordenite [17,18] and zeolites NaX and NaY [19,20]) have often been the target of the investigations, because they show a high capacity for the PV dehydration of organic liquid mixtures (e.g., short and long-chain alcohols, DMF, THF, . . .). Currently, commercial PV units based on zeolite NaA membranes are used at an industrial level and are routinely able to dehydrate a variety of solvents [21].

Despite the great number of studies focusing on zeolite membrane preparation and PV performance, hardly any accurate description of the mass transfer through these membranes in the PV process has been proposed in the literature. Modeling the PV process is something relevant not only for a proper understanding of the mechanisms involved, but also for the design of PV modules. On the contrary, several models have been presented for polymeric membranes [22]. The first approach to describe the PV process [3] assumed the existence of two phases inside the membrane, namely, a ''solution phase'' next to the feed/membrane interface and a ''vapor phase'' on the other side, so that the permeating molecules experienced their main resistance to permeation only in the vapor phase.

More generally and phenomenologically, the PV process through polymeric membranes is often described by the solution–diffusion model [3,23], which concerns three successive steps: (1) selective solution of the species in the liquid mixture at the feed/membrane interface, (2) diffusion through the membrane and (3) desorption at the membrane/permeate interface. The diffusion process (2) is usually accounted for by Fick's First Law with concentration-dependent diffusivities [22]. Recently, Bowen et al. [24] and Ortiz et al. [25] successfully applied the solution–diffusion model, respectively, for the description of the PV performance of highly hydrophobic Ge-ZSM-5 zeolite membranes (germanium substituted, MFI structure) and for the dehydration of ketonic and THF mixtures (water content 1–8 wt.%) with zeolite NaA membranes. While the former described the diffusion process with constant fickian diffusivities, the latter used an empirically improved version of that model by taking into account a decreasing exponential dependency on the surface coverage or fraction of the occupied centers on the adsorbent. However, this model fails to predict the PV performance of zeolite membranes for liquid mixtures with high water content [16]. It is well known that at low temperature, mass transfer through

zeolite pores occurs by surface diffusion through an adsorption–diffusion mechanism [16,26], that is, adsorbed molecules diffuse along the surface of zeolite pores by jumping from site to site, given by the chemical potential gradient within the pores. The dehydration of organic solvents by hydrophilic zeolite membranes usually takes place on the grounds of adsorption differences between water and the solvent [10].

In an attempt to provide an insight into the mechanisms that govern the PV process, the present paper is devoted to describing the dehydration performance a zeolite NaA membrane prepared in our laboratory with high selectivity and water flux towards the separation of ethanol/water mixtures. To this end, the generalized Maxwell–Stefan theory (GMS), traditionally applied for the description of gas permeation through MFI zeolite membranes, has been extended to PV to account for the selective water removal shown by hydrophilic zeolite membranes.

2. Experimental

2.1. Membrane synthesis

The membrane used in this study consisted of a continuous active layer (thickness: ~30 μm) of randomly oriented and intergrown zeolite NaA crystals located in the inner surface of a porous tubular α-alumina support (Inocermic, Hermosdorf, Germany). Both ends of the support (7 mm i.d. and 10 mm o.d.) were subjected to enameling to define a permeation length of ~5 cm (inner surface: 1.25×10^{-3} m^2). The zeolite NaA layer was grown by seeded hydrothermal synthesis (secondary-growth method). The inner surface of the support was first coated with A-type zeolite crystals (2 μm) supplied by Industrias Químicas del Ebro (IQE, Zaragoza, Spain) by means of a cross-flow filtration technique. Subsequently, crystallization was carried out in two cycles using a semi-continuous system at 363–373 K for periods of 5 h with a milky-like gel enriched with Al nutrient. A fixed volume of the gel (6.3 mL) was refreshed from a preheated reservoir kept at 5–10 bar with dry N_2 by the action of a set of electro-pneumatic valves at a renewal rate of 1/7 min^{-1}. The membrane displayed low N_2 permeation (1.58×10^{-9} mol m^{-2} s^{-1} Pa^{-1}) and a good PV performance for the separation of a 92:8 wt.% ethanol/water mixture at 323 K and with a permeate pressure kept <2 mbar (selectivity towards water: 700, total flux: 0.48 kg m^{-2} h^{-1}). Relevant data concerning both seeding and synthesis processes are summarized in Table 1. For further details see Pera-Titus et al. [11,27].

Table 1
List of seeding and synthesis conditions for zeolite NaA membrane preparation

Seeding	
Technique	Cross-flow filtration
Support	α-Alumina
Mean pore size (μm)	1.9
Porosity	0.16
Mean crystal size (μm)	2
Concentration in suspension (ppm)	20
pH	10
Transmembrane pressure (bar)	1
Feed flow rate (L min^{-1})	5.5
Hydrothermal síntesis	
Technique	Semi-continuous
Gel composition (molar) (Al_2O_3:SiO_2:Na_2O:H_2O)	1.0:1.8:3.9:270
Temperature (K)	363–373
Synthesis time (h)	5
Number of cycles	2
Renewal rate (min^{-1})	1/7

2.2. PV experiments

A set of steady-state PV experiments with ethanol/water mixtures was performed by means of a conventional laboratory-scale PV plant. The details of the experimental set-up are described elsewhere [11]. The PV experiments were carried out by pumping (300 mL min^{-1}) the ethanol/water liquid mixtures contained in the feed tank through the PV membrane module (inside of the tube) placed in a temperature-controlled oil bath and recirculated to the feed tank. The retentate temperature and pressure were monitored, respectively, by a thermocouple (±1 K) and a manometer (±0.1 bar). Samples were taken at the feed inlet and retentate outlet of the membrane module by two needle valves.

The permeate pressure was measured using a digital vacuum gauge (±0.5 mbar) (Schlee Gmbh & Co. V-D3, Witten, Germany) installed in the line connecting the PV module and the condenser. The condenser consisted of a set of cold traps cooled with liquid nitrogen and located among the membrane module and the oil vacuum pump (Telstar, Sabadell, Spain). Two cold traps were set in parallel allowing the experiments to be carried out in continuous mode and in series with an additional cold trap to prevent the oil pump from succumbing to any vapor contamination. Both the feed and the collected liquid were analyzed in a gas chromatograph (HP 6890 series equipped with a TCD detector, USA). The selectivity of the membrane was calculated as the ratio of the weight fractions of water and ethanol in the permeate side to that in the feed (i.e $\alpha_{W/E} = (Y_W/Y_E)/(X_W/X_E)$). The final values given correspond to the mean of two to six replicates measured after at least 4 h of stabilization. A summary of the experimental conditions surveyed in this study is given in Table 2.

For all the experiments involving higher temperatures (363 K) and higher water concentrations (10–60 wt.%), the flux permeated was <3% of the retentate flow because of the low

Table 2
Experimental conditions for PV experiments with ethanol/water mixtures

Feed flow (mL min^{-1})	300
Water composition (wt.%)	1–60
Temperature (K)	303–363
Relative feed pressure (bar)	0–7
Permeate vapor pressure (mbar)	1–70
Stabilization time (h)	2–4
Experimental time (h)	1–3
Number of replicates	2–6

membrane area used (1.26×10^{-3} m^2). The composition of the feed and retentate were also measured several times to verify constancy in composition. Moreover, previous experiments were conducted at different flow rates to ascertain the presence of either radial or axial gradients in the membrane tube.

3. Theory

3.1. Mass transfer through a composite zeolite membrane: adsorption–diffusion model

Fig. 1 shows a schematic representation of the PV process in a zeolite NaA membrane. The membrane is visualized as a system where a liquid mixture is put into contact with a zeolite thin layer grown onto a much thicker porous support. If both the feed (retentate) and the permeate volumes are considered to be well mixed, the mass transfer must be wholly ascribed to the membrane (zeolite layer + support). Moreover, mass transfer within the zeolite layer seems to be rate limiting, that is, the support (mass transfer governed by a Knudsen diffusion mechanism [28]) does not offer much resistance to the overall mass transfer through the whole membrane. In the present study, we found that the pressures at the membrane/support interface are only slightly higher (up to 10%) than those of the bulk vapor permeate. This point implies support resistances up to 5% of the overall.

Furthermore, according to Nomura et al. [26], on the grounds of its polycrystalline nature, the zeolite layer is viewed as an assembly of zeolite grains (see Fig. 1) that might include two different kinds of pores: (1) intracrystalline or zeolite pores and (2) intercrystalline or non-zeolite pores. The former consist of subnanometric pores (mean pore size <1 nm) defined by the zeolitic crystalline lattice, while the latter might be regarded as grain boundaries in the borderline defined between two

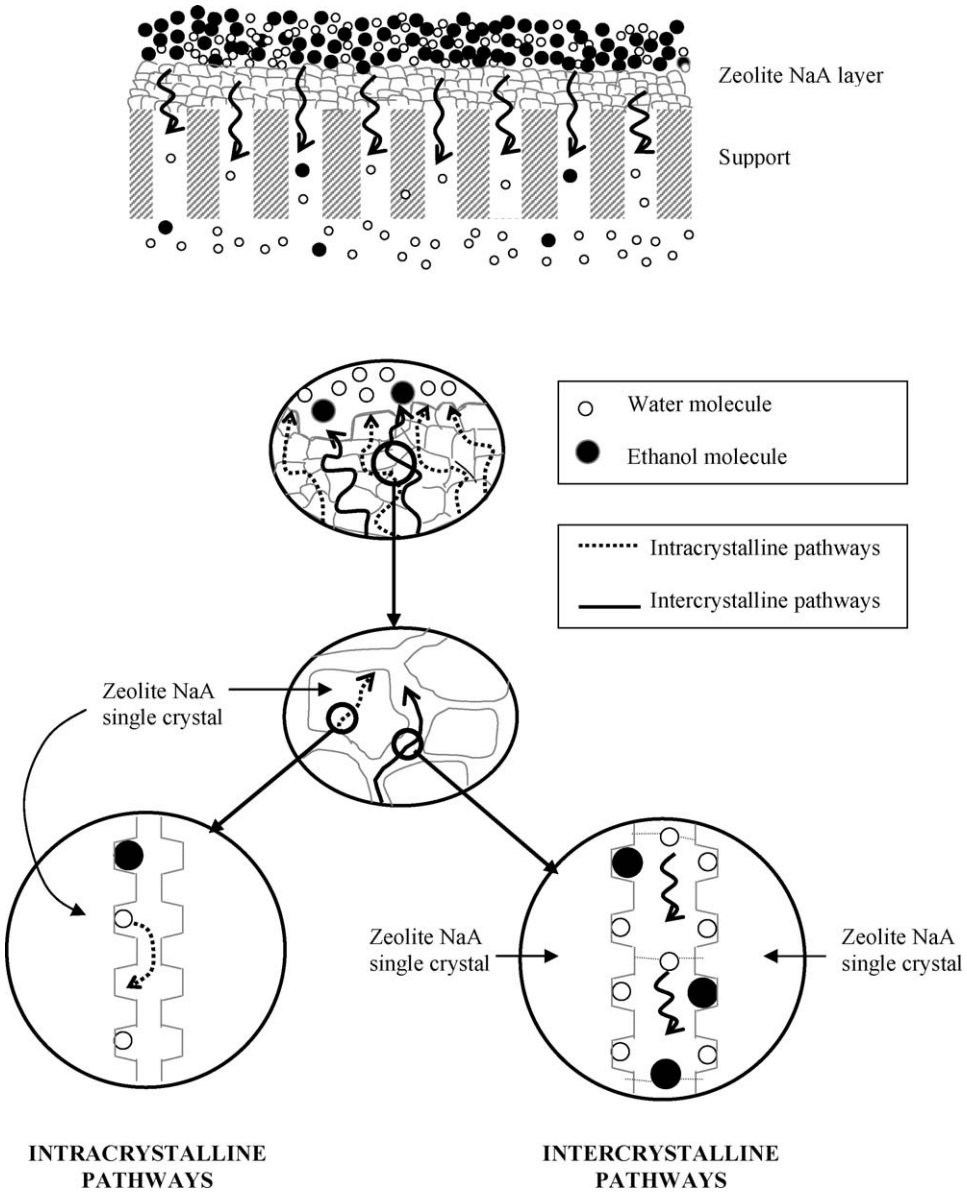

Fig. 1. Schematic representation of the intracrystalline and intercrystalline pathways for mass transfer in the zeolite layer.

adjacent zeolite single crystals. Both pores might involve different pathways for mass transfer owing to their different structure. In the present study, evidence for the presence of non-zeolitic pores was found from a SF_6 permeation experiment (permance: 8.35×10^{-10} mol m^{-2} s^{-1} Pa^{-1}; N_2/SF_6 selectivity: 1.89). Since SF_6 has a kinetic diameter of 0.55 nm, a number of non-zeolite pores with a mean pore size higher than this value must be present in the zeolite layer. In this work, we use a set of equations to model the zeolite pores without distinction between intracrystalline or intercrystalline pores. Therefore, the calculated model parameters, deduced from the experimental data, will be affected by the relative amount of intercrystalline pores.

3.2. Mass transfer in the zeolite layer

3.2.1. Generalized Maxwell–Stefan theory

The generalized Maxwell–Stefan theory (GMS) earlier developed and reviewed by Krishna and Wesseling [28,29] and Van den Broeke and Krishna [30] provides an adequate basis for the description of multicomponent mass transfer of adsorbed species in subnanometric microporous materials (mean pore size <1 nm) (e.g., zeolites) when surface diffusion along the surface within the adsorbent pores is the rate limiting process. In the last few years, the Maxwell–Stefan formulation has revealed as a convenient and amenable way to interpret and simulate the permeation performance of hydrocarbons through MFI membranes [31–34].

Since the size of the permeating molecules are of the same order as that of the micropores, the GMS theory conventionally assumes that movement of a species is caused by a driving force which is balanced by the friction experienced from each other and its surroundings [28]. Taking the gradient of chemical potential for each species i, $-\nabla\mu_i$, as the driving force and treating vacancy sites as active species, the general form of the GMS equations applied to surface diffusion is given by Eq. (1).

$$-\frac{\theta_i}{RT}\nabla_T\mu_i = \sum_{\substack{j=1 \\ j\neq i}}^{C} \theta_j \frac{(\theta_j N_i^S - \theta_i N_j^S)}{\rho_p q_{M,j} Đ_{ij}^S} + \frac{N_i^S}{\rho_p q_{M,i} Đ_{iV}^S} i, \quad j = 1,2,\ldots,C \tag{1}$$

The first term on the right-hand side in Eq. (1) reflects the friction exerted between adsorbed molecules, while the second one represents the friction between a molecule and the pore wall. Both interactions can be modeled, respectively, by means of MS counterexchange diffusivities, $Đ_{ij}^S$ and MS surface diffusivities, $Đ_{iV}^S$. For zeolite topologies with high connectivity (e.g. LTA), the counterexchange coefficient $Đ_{ij}$ can be expected to be high (i.e. $Đ_{ij} \to \infty$), which implies that the mobility of adsorbed species **i** is not expected to contribute to the mobility of **j** [28,35]. For this particular situation, the first term on the right-hand in Eq. (1) vanishes. It should be noted that the MS formalism involves the use of MS diffusivities instead of fickian diffusivities, because surface fluxes are related to chemical potential gradients instead of partial pressure gradients. Surface diffusion in microporous materials constitutes a temperature-activated process that takes place by a sequence of jumps between nearby regions of low potential energy or sites [28,36,37].

On the other hand, the chemical potential gradient can be related to the gradient of surface coverage by a matrix of thermodynamic factors, Γ_{ij} [28,35]

$$\frac{\theta_i}{RT}\nabla\mu_i = \sum_{j=1}^{C}\Gamma_{ij}\nabla\theta_j \quad \text{where}$$

$$\Gamma_{ij} \equiv \theta_i \frac{\partial \ln p_i}{\partial\theta_j} i, j = 1,2,\ldots,C \tag{2}$$

The form of the thermodynamic factors is determined by the form of the multicomponent adsorption isotherm chosen to relate the surface coverage, θ_i, to the partial pressure. In this study, the extended Langmuir isotherm was used (Eq. (3))

$$\theta_i = \frac{q_i}{q_{M,i}} = \frac{K_i p_i}{1 + \sum_{j=1}^{C} K_j p_j} \tag{3}$$

The extended Langmuir isotherm constitutes the simplest mathematical function to account for multicomponent adsorption, which only shows thermodynamic consistency if the adsorbing species have the same molar saturation loading, $q_{M,i}$ [38]. However, other models based on the ideal adsorbed solution theory (IAST) developed by Myers and Prausnitz [38] and further modifications such as the real adsorbed solution theory (RAST) [39] and the predictive real adsorbed solution theory (PRAST) [40] might be more adequate to describe multicomponent adsorption equilibrium. In this way, Kapteijn et al. [41] derived expressions to account for the performance of silicalite-1 membranes towards the separation of hydrocarbons with different molar saturation loadings by combining the Maxwell–Stefan diffusion model with the IAST model.

Furthermore, MS surface diffusivities can be reduced due to the interactions between adsorbed species in the solid [28]. If one molecule can only migrate from one site to another one as long as the latter is vacant and if the extended Langmuir isotherm is adopted, MS surface diffusivities adopt the form given by Eq. (4) [37]

$$Đ_{iV}^S(\theta_V) = Đ_{iV}^S(0)\theta_V \tag{4}$$

MS surface diffusivities at zero coverage, $Đ_{iV}^S(0)$ are assumed to be temperature-dependent according to the Arrhenius equation, that is:

$$Đ_{iV}^S(0) = A_i^S \exp\left(-\frac{E_i^S}{RT}\right), \tag{5}$$

where the activation energy of each species, E_i^S, is related to the energy barrier the aforementioned species has to overcome to jump from one site to another that is vacant in its neighborhood.

3.2.2. Application of GMS theory to PV of ethanol/water mixtures

Eq. (1) can be applied to describe the steady-state PV performance of zeolite NaA membranes towards the dehydration

of ethanol together with the extended Langmuir isotherm to account for binary adsorption equilibrium (adsorption–diffusion model). Although the thermodynamic requirement of equal molar saturation loadings for each adsorbing species is not actually satisfied for this system (15.0 mol kg^{-1} versus 4.5 mol kg^{-1} for water and ethanol, respectively [15]), a constant saturation loading has been assumed along this study (i.e. $q_{M,W} = q_{M,E} = q_M$, with mean value ~10 mol kg^{-1}) for competitive adsorption of water and ethanol. In this case, this assumption tends to overestimate the ethanol loading and underestimate the water loading and, consequently, will tend to underestimate the ethanol diffusivity and overestimate the water diffusivity. However, these drawbacks are in some measure compensated by the mathematical simplicity and the successful of the model in predicting the PV process. Furthermore, the extended Langmuir analysis does not allow for the complete or partial exclusion of the entropically less favored species (ethanol in this case) that can occur at high loadings according to Krishna [42]. However, a more proper description involving the Adsorbed Solution Theory along the same lines as outlined by Kapteijn et al. [41] might provide a more elaborated description of the binary diffusion process in the special case where different molar saturation loadings are taken into account.

Furthermore, under the additional assumptions that (1) mass transfer of water and ethanol through a zeolite NaA layer (both through zeolite and non-zeolite pores) is the rate limiting step, (2) the process occurs under the assumption that $Đ_{ij} \to \infty$, (3) surface diffusion takes place preferentially between α- rather than β-cages because of the hindering effect of the latter [43] (the kinetic diameters of water and ethanol, 0.26 and 0.52 nm [16], respectively, are of the same order as the window openings between α-cages, 0.41 nm [41]) and (4) water is preferentially adsorbed in the zeolite cavities compared to ethanol (i.e. $\theta_w \gg \theta_E$ or $K_W a_w \gg K_E a_E$) on the grounds of the hydrophilic character of zeolite NaA, Eq. (1) is transformed into Eqs. (6) and (7) for both water and ethanol, respectively

$$N_W^S = -\rho_s q_M M_W Đ_W^S(0) \nabla\theta_W \tag{6}$$

$$N_E^S = -\rho_s q_M M_E Đ_E^S(0)\{(1-\theta_W)\nabla\theta_E + \theta_E \nabla\theta_W\} \tag{7}$$

It should be noted that the form of Eq. (6) indicates that water might permate according to a pseudo-fickian process. Moreover, assuming that mass transfer only takes place along the Z-direction perpendicular to the membrane plane and that pores are non-tortuous under the boundary conditions:

$$Z = 0, \theta_W = \theta_{W,L}, \theta_E = \theta_{E,L}$$

$$Z = \ell, \theta_W = \theta_{W,v}, \theta_E = \theta_{E,v},$$

the set of Eqs. (6) and (7) admits an analytical solution through the convenient definition of non-dimensional water and ethanol surface fluxes, $(N_W^S)^* = N_W^S \ell / \rho_s q_M M_W Đ_W^S(0)$ and $(N_E^S)^* = N_E^S \ell / \rho_S q_M M_E Đ_E^S(0)$, respectively. The final equations for surface fluxes correspond to Eqs. (8) and (9)

$$N_W^S = \frac{\rho_S q_M M_W Đ_W^S(0)}{\ell}(\theta_{W,L} - \theta_{W,v}) \tag{8}$$

$$N_E^S = \frac{\rho_S q_M M_E Đ_E^S(0)}{\ell}(1-\theta_{W,L})(\theta_{E,L} - \theta_{E,v}) + \frac{M_E Đ_E^S(0)}{M_W Đ_W^S(0)}\theta_{E,L} N_W^S, \tag{9}$$

while the selectivity towards water separation becomes Eq. (10)

$$\alpha_{W/E} = \frac{X_E}{X_W}\frac{N_W}{N_E} = \frac{X_E}{X_W}\frac{M_W}{M_E}\frac{Đ_W^S(0)}{Đ_E^S(0)}\left[\frac{(\theta_{W,L} - \theta_{W,v})}{\theta_{E,L}(1-\theta_{W,v}) - \theta_{E,v}(1-\theta_{W,L})}\right] \tag{10}$$

It should be stressed that the set of Eqs. (8) and (9) is identical to the one that might be obtained from the analytical general solution found by Krishna and Baur [44] for a binary system under the same assumptions. Regarding the form of both equations, while water surface flux is only conjugated to its own driving force (surface coverage gradient), ethanol flux appears to be also coupled to water surface flux (second term on the right-hand side). In addition, water and ethanol surface coverages at both feed/and permeate/membrane surfaces can be translated into partial pressures using the extended Langmuir isotherm, where partial pressures at the former surface is assumed to be at equilibrium with the liquid mixture according to Eqs. (11) and (12)

$$p_{W,L} = \gamma_W(x_{W,L}, T) x_{W,L} P_W^0 = a_{W,L} P_W^0 \tag{11}$$

$$p_{E,L} = \gamma_E(x_{E,L}, T) x_{E,L} P_E^0 = a_{E,L} P_E^0 \tag{12}$$

where the activity coefficients, γ_i, can be estimated by the UNIFAC method [45]. Eventually, Eqs. (8) and (9) become Eqs. (13) and (14) to describe the adsorption–diffusion process

$$N_W^S = \frac{\rho_S q_M M_W Đ_W^S(0) K_W^S P_W^0}{\ell} \times \left(\frac{a_{W,L}}{1 + K_W^S a_{W,L} P_W^0} - \frac{p_{W,v}/P_W^0}{1 + K_W^S p_{W,v}}\right) \tag{13}$$

$$N_E^S = \frac{\rho_S q_M M_E Đ_E^S(0)}{\ell} \times \left(\frac{1 + K_{E,L}^S a_{E,L} P_E^0}{1 + K_W^S a_{W,L} P_W^0}\right)\left(\frac{K_{E,L}^S a_{E,L} P_E^0}{1 + K_W^S a_{W,L} P_W^0} - \frac{p_{E,v}}{1 + K_W^S p_{W,v}}\right) + \frac{K_E^S a_{E,L} P_W^0}{(1 + K_W^S a_{W,L} P_W^0)} \frac{M_E Đ_E^S(0)}{M_W Đ_W^S(0)} N_W^S, \tag{14}$$

The mathematical form of Eq. (13) allows the definition of a water permeability, Q_W^S, which can include three major contributions to water mass transfer in the PV process: (1) MS surface diffusivity of water at zero coverage, (2) water adsorption constant and (3) saturation vapor pressure of water,

that is:

$$Q_{\mathrm{W}}^{\mathrm{S}} = \rho_{\mathrm{S}} q_{\mathrm{M}} M_{\mathrm{W}} Đ_{\mathrm{W}}^{\mathrm{S}}(0) K_{\mathrm{W}}^{\mathrm{S}} P_{\mathrm{W}}^{0} \quad (15)$$

Since all these contributions to water permeability are temperature-dependent, it can be wholly regarded as an activated process according to Eq. (16)

$$Q_{\mathrm{W}}^{\mathrm{S}} = \rho_{\mathrm{S}} q_{\mathrm{M}} M_{\mathrm{W}} Đ_{\mathrm{W}}^{\mathrm{S}}(0) K_{\mathrm{W}}^{\mathrm{S}} P_{\mathrm{W}}^{0} = A_{\mathrm{W,eff}}^{\mathrm{S}} \exp\left(\frac{-E_{\mathrm{W,eff}}^{\mathrm{S}}}{RT}\right), \quad (16)$$

where $E_{W,\mathrm{eff}}^{S}$ and $A_{W,\mathrm{eff}}^{S}$ are considered, respectively, as an effective activation energy and pre-exponential factor. According to Eq. (15), both parameters might include three contributions as it is outlined in Eqs. (17) and (18)

$$E_{\mathrm{W,eff}}^{\mathrm{S}} = E_{\mathrm{W}}^{\mathrm{S}} + \Delta H_{\mathrm{W}}^{0} + RA \quad (17)$$

$$A_{\mathrm{W,eff}}^{\mathrm{S}} = \rho_{\mathrm{S}} q_{\mathrm{M}} M_{\mathrm{W}} A_{\mathrm{W}}^{\mathrm{S}} K_{\mathrm{W}}^{\mathrm{S}}(T_{\mathrm{ref}}) \exp(B), \quad (18)$$

where parameters A and B belong to the Antoine Equation ($\ln(P_{\mathrm{W}}^{0}) = B - A/T$), which accounts for the evolution of saturation vapor pressure with the temperature. For water in the temperature range 293–363 K, $A = 5300\ \mathrm{K}^{-1}$ and $B = 20.95$.

3.3. Fitting of experimental data to the adsorption–solution model

Table 3 lists the relevant membrane parameters used in Eqs. (13) and (14) for the prediction of water and ethanol surface fluxes. A least-square non-linear optimization method, based on the Levenberg–Marquardt algorithm, was used to adjust the kinetic parameters of the model by the comparison of predicted and experimental water and ethanol surface fluxes. In the fitting process, MS surface diffusivities and adsorption constants were expressed according to Eqs. (19) and (20)

$$D_i(0)(T) = D_i(0)(T_{\mathrm{ref}}) \exp\left[\frac{-E_i^{\mathrm{S}}}{R}\left(\frac{1}{T} - \frac{1}{T_{\mathrm{ref}}}\right)\right] i = \mathrm{W}, \mathrm{E} \quad (19)$$

$$K_i(T) = K_i(T_{\mathrm{ref}}) \exp\left[\frac{-\Delta H_i^{0}}{R}\left(\frac{1}{T} - \frac{1}{T_{\mathrm{ref}}}\right)\right] \quad (20)$$

The fitting process was done in two subsequent steps. Firstly, water parameters were adjusted by fitting experimental water fluxes to Eq. (13). Subsequently, ethanol parameters were adjusted by fitting experimental ethanol fluxes to Eq. (14).

Table 3
Membrane parameters used for the modeling

Density of zeolite NaA (kg m^{-3})	1900
Molar saturation loading (mol kg^{-1})	10*
Thickness of the zeolite layer (μm)	~30**
Inner surface area of the layer (m^2)	1.26×10^{-3}

* Mean value between those of water and ethanol.
** Determined by S.E.M.

4. Results and discussion

4.1. General trends for total flux and selectivity towards water separation

4.1.1. Effect of feed (retentate) pressure

The effect of feed (retentate) relative pressure in the range 0–7 bar on the total flux and selectivity towards water separation by PV from an ethanol/water mixture (92:8 wt.%) at 323 K and for a vapor permeate pressure kept <2 mbar is depicted in Fig. 2. As can be seen, while the total flux tends to rise slightly with feed relative pressure, water/ethanol selectivity shows a quite dramatic reduction. Although the membrane shows high quality towards water dehydration, these trends confirm the presence of a reduced number of large non-zeolite pores in the zeolite layer, which might correspond to cracks or pinholes. In fact, the study of the functional dependence of the total flux and selectivity of a composite zeolite membrane with feed relative pressure might provide valuable data for the quantification and characterization of non-zeolite pores. In this way, a greater dependence of both properties on the feed relative pressure might reveal a higher number or the presence of larger non-zeolite pores.

It should be emphasized that non-zeolite pores, especially the largest ones, might contribute to the PV performance of the membrane even at very low feed relative pressures, because the permeate vapor is kept at <2 mbar in most of the experiments and a net pressure driving force (at least ~1 bar) exists within the membrane. However, to reduce their contribution, most of the experiments were carried out at a low feed relative pressure (0.6 bar), but higher than atmospheric pressure to prevent the liquid feed from vaporization at higher temperatures (i.e. 363 K).

4.1.2. Effect of feed composition

Fig. 3 shows the effect of the feed composition and temperature on the total flux and selectivity towards water

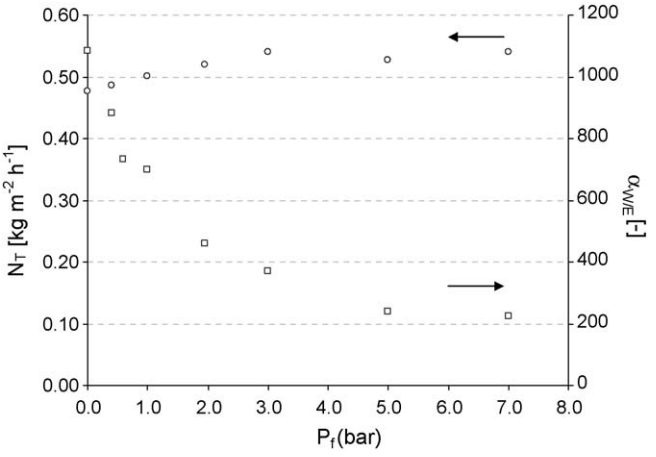

Fig. 2. Evolution of the total flux and selectivity with the feed pressure (relative) for the PV separation of ethanol/water mixtures by the membrane prepared. Experimental conditions: $X_{\mathrm{H_2O}} \approx 8.4$–9.0 wt.%; $T = 323$ K; $P_{\mathrm{v}} = 1$–2 mbar. Standard deviation ≤5% for total flux and ≤10% for selectivity. Open cycles and squares refer, respectively, to the total flux and selectivity of the membrane.

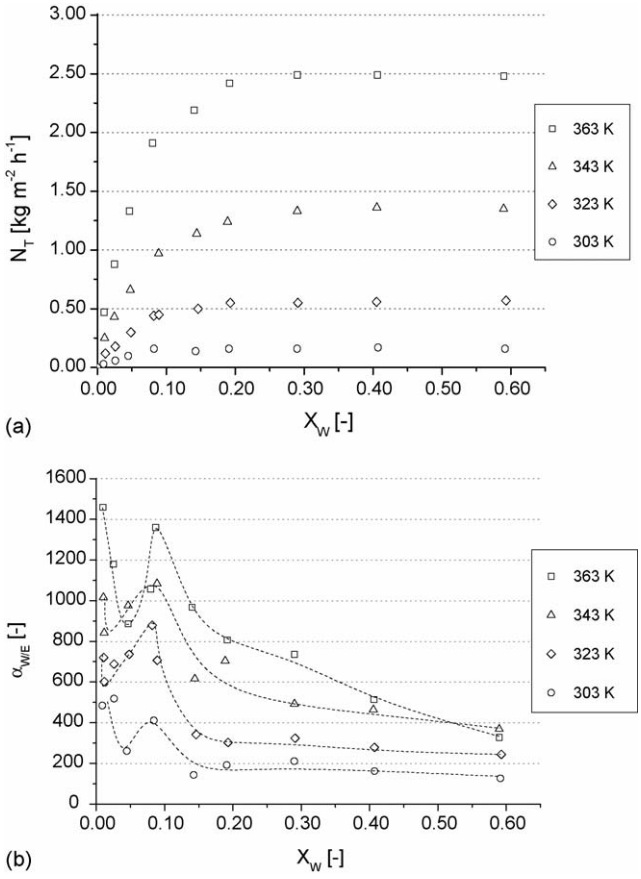

Fig. 3. Evolution of (a) total flux and (b) selectivity with feed composition. Experimental conditions: T = 303–363 K, P_v = 1 mbar, P_f = 0.6 bar (relative). Standard deviation ≤2% for total flux and ≤4% for selectivity. Dashed lines refer to the general trends observed for selectivity.

separation from ethanol/water mixtures. The total flux is observed to increase with water fraction for all the temperatures under study (see Fig. 3a). At low water fractions (<8–10 wt.%), the total flux tends to show a linear increase with the water fraction, while at water fractions beyond the 20–30 wt.% this flux tends to a constant asymptotic values. These observations could be ascribed to the great affinity for water that zeolite NaA shows owing to its marked hydrophilic character. Thus, the zeolite active layer might preferentially adsorb water over ethanol and as a result, water flux through the membrane might remain high and constant for high water fractions. On the other hand, the decrease in total flux observed at water fractions <8–10% could be related to the decrease in the water driving force according to Eq. (13).

In fact, the trend depicted in Fig. 3a is similar to the form of the Langmuirian adsorption isotherm for water [15], which actually relates surface coverage with partial pressure at equilibrium with the solid. This analogy might imply a relevant contribution of water adsorption equilibrium at the liquid feed/membrane surface on the actual PV performance of the membrane in the way outlined by Eq. (13).

On the other hand, Fig. 3b shows the effect of feed composition on the selectivity of the membrane for the temperature range under study. As can be seen, the selectivity tends to show a maximum with the water fraction in the range 5–10 wt.% in agreement with the results reported by Okamoto et al. [15], with values up to 1400 ± 70 at 363 K for the present study. Such high selectivities reflect the great contribution of zeolite pores to discrimination between water and ethanol molecules. However, according to the trends for total flux and selectivity outlined in Fig. 2, the contribution of non-zeolite domains to total mass transfer cannot be ruled out.

The presence of a maximum in the plot of selectivity with feed composition might be explained according to the definition of selectivity (see Section 2.2). For water fractions <10 wt.%, water and ethanol fluxes show a dramatic rise with the feed composition, which implies a rise of selectivity values. Otherwise, beyond water fractions of 10 wt.%, water and ethanol fluxes tend to show steady values, which involves the reduction of selectivity with water fraction according to the function $[(1 - X_W)/X_W]$.

4.1.3. Effect of temperature

Fig. 4 shows the effect of temperature on the water flux and selectivity of the membrane for different feed compositions. As can be seen in Fig. 4a, water flux shows values up to 2.50 ± 0.10 kg m^{-2} h^{-1} at 363 K, which are somewhat lower than those reported in the literature [15,16] and tends to rise with temperature according to an Arrhenius plot, which reveals the activated nature of the permeation process through zeolite crystals. Therefore, Knudsen diffusion, often observed for gas

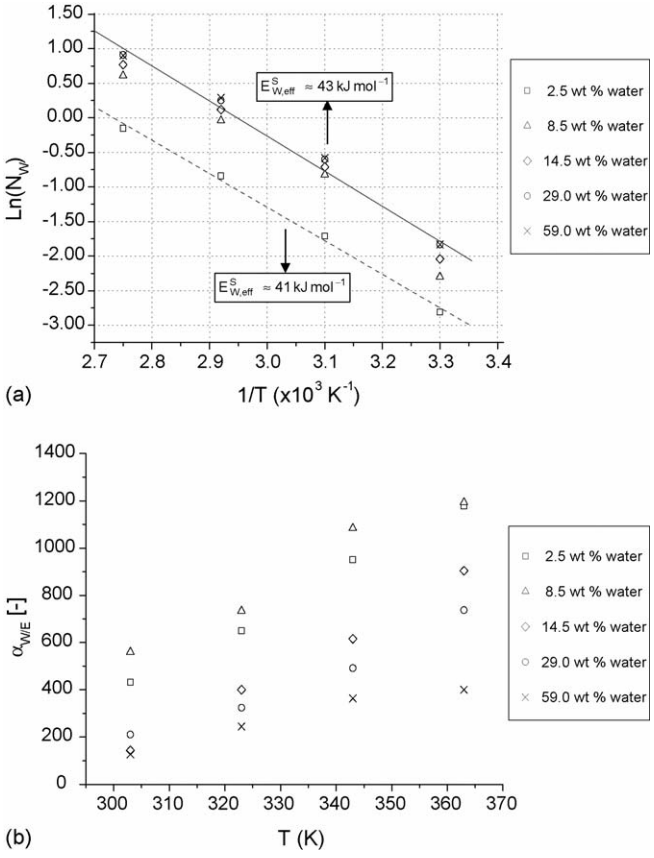

Fig. 4. Evolution of (a) total flux and (b) selectivity with temperature. Experimental conditions: X_{H_2O} ≈ 2.5–59 wt.%, P_v = 1 mbar, P_f = 0.6 bar (relative).

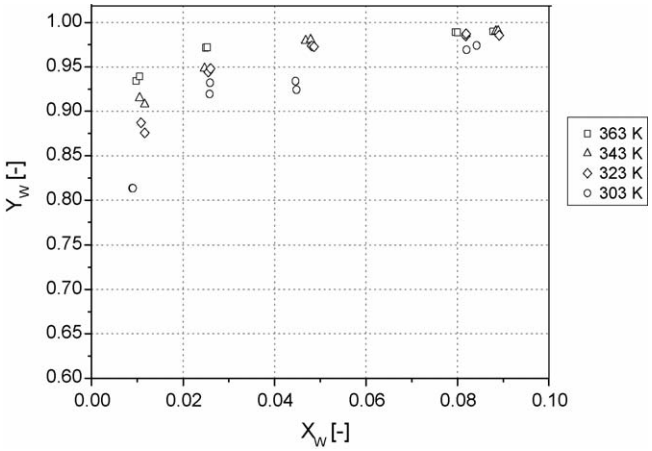

Fig. 5. Permeate composition vs. feed composition in the separation of ethanol/water mixtures.

permeation through zeolite A crystals, might be ruled out as the dominating mass transfer mechanism in the current membrane, since a decrease with $T^{-1/2}$ should be expected [28].

The effective activation energy for water flux, $E^{S}_{W,eff}$, computed in this study for the system ethanol/water lies in the range 41–43 kJ mol^{-1} for feed water fractions varying from 2.5–59 wt.%, which is of the same order as that reported by Shah et al. [16], 51–52 kJ mol^{-1}, for feed water fractions varying from 10–100 wt.% and 35 kJ mol^{-1} reported by Okamoto et al. [15] for feed water fractions of 10 wt.%. This result reflects that once water molecules enter the zeolitic structure, they diffuse in the usual manner with the same activation energy. Although the effective activation energy remains practically invariable for the range of feed water fractions studied, it should be noted that the intercept of the lines with the ordinate axis at low feed water fractions (i.e. 2.5 wt.%) tends to be lower than that found in the range 8.5–59.0 wt.%. This observation might be ascribed to the dramatic reduction of water activity in the feed, thus causing a reduction of water driving force and therefore a lowering of the water flux.

On the other hand, the selectivity of the membrane towards water separation also tends to rise with temperature in the range 303–363 K (see Fig. 4b), namely better separations can be achieved at higher temperatures. In fact, this trend is opposite to that reported by Okamoto et al. [15] for the separation of ethanol/water mixtures by PV and by Van den Graaf et al. [31] for gas separation by MFI zeolite membranes. The discrepancy between these trends might be ascribed to the presence of a reduced number of non-zeolite domains in the zeolite layer prepared in this work. A temperature rise might enhance water transfer through the zeolite layer, thus compensating for the effect of ethanol transfer through non-zeolite pores and giving rise to a global increase of the selectivity of the membrane.

4.1.4. Trend of permeate composition with feed composition (Y_W–X_W curve)

Fig. 5 shows the evolution of the feed water fraction on the composition of the vapor permeate composition (Y_W–X_W curve) for the temperature range under study. As can be seen, because water/ethanol selectivities are very high, the permeate is enriched with water. It should be mentioned that the composition of the permeates was >90 wt.% for feed water fractions <2–4 wt.%. The membrane is more enriched in water at higher temperatures, in agreement with the positive effect exerted by temperature to selectivity indicated in Fig. 4b.

4.2. Description of the PV performance in zeolite membranes

4.2.1. Correlations for surface fluxes and selectivity

In Fig. 6a and b both experimental water and ethanol surface fluxes obtained in the conditions indicated in Table 3 are compared to fluxes adjusted to Eqs. (13) and (14). In both cases, excellent fits are obtained, thus revealing that the MS formulation (adsorption–diffusion model) seems to provide a good basis for the description of the PV process for the separation of ethanol/water mixtures with zeolite NaA membranes. Moreover, experimental selectivities also agree fairly well with those predicted by the model (see Fig. 6c). The values for the parameters fitted and the statistics of the fits are summarized in Tables 4 and 5, respectively.

On the other hand, experimental and fitted trends for both water and ethanol fluxes with feed composition are depicted, respectively, in Fig. 7a and b. As can be seen, the trend for experimental water flux resembles that of the total flux (see Fig. 3a) owing to the high selectivities towards water separation that these membranes show. Water flux does not appear to be altered by the presence of ethanol, except for low water activities. However, the ethanol flux is strongly reduced by the presence of water in the liquid feed. This latter trend could be ascribed to the reduction of selectivity with the feed composition for water fractions higher than 10 wt.%. The set of Eqs. (13) and (14) reproduce successfully the trends outlined in Fig. 7a and b, which confirms the important role of water adsorption on the zeolite layer in the PV process, that is, the separation behavior of the membrane seems to be governed by differences in adsorption.

4.2.2. Fitting the trend of water flux with permeate pressure

Fig. 8 shows the experimental and fitted trends for water flux with the vapor permeate vacuum pressure. As can be seen, water flux is affected by the vapor permeate pressure, being it reduced with a rise of the permeate vapor pressure. This trend seems to be fairly well described by the Maxwell–Stefan approach. In this way, permeate pressure kept under vacuum might allow the removal of adsorbed molecules on the permeate/membrane interface, thus allowing the presence of a surface coverage gradient within the membrane and therefore mass transfer. The surface coverage at this surface might increase with a rise of the vapor permeate pressure, thus reducing the surface coverage driving force within the membrane and consequently reducing dramatically the total flux through the membrane.

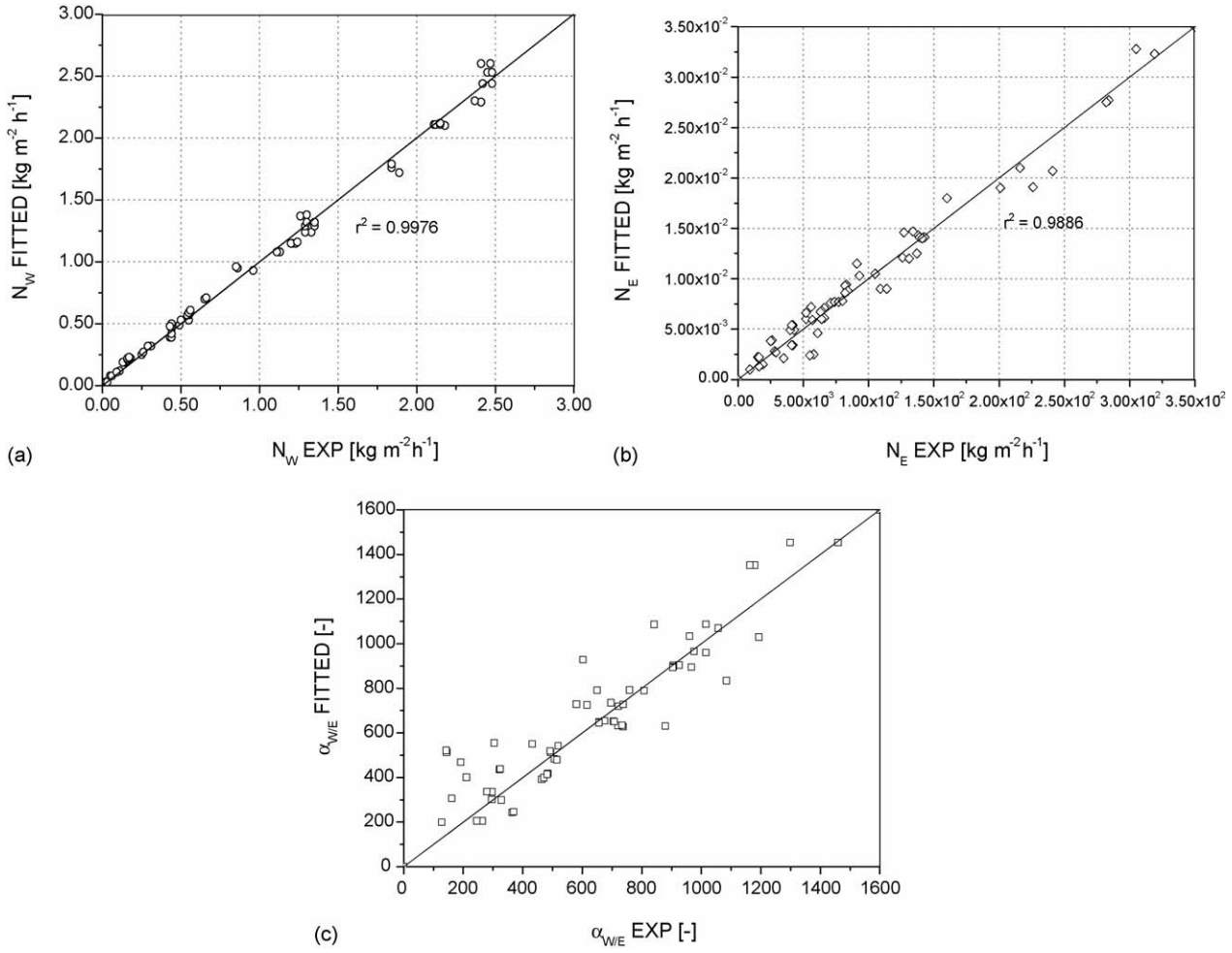

Fig. 6. Comparison between experimental and fitted trends for (a) water flux, (b) ethanol flux and (c) selectivity towards water separation. Experimental conditions in Table 2.

4.2.3. Adsorption–diffusion versus Solution–diffusion model

Fig. 9 shows the trends for water and ethanol fluxes with the driving force $\Delta p_i = a_{i,\mathrm{L}} P_i^0 - p_{i,\mathrm{v}}$ used for in the solution–diffusion model at 363 K. As can be seen, the solution–diffusion model fails to predict the PV behavior of zeolite NaA membranes, because the experimental fluxes do not show a linear trend with the pressure driving force. It should be mentioned that water fluxes show a linear trend with its driving force for values comprised between 0 and 30,000 Pa (water fractions in the range 0–8.5 wt.%), but beyond this 30,000 Pa, important deviations from the linear trend are observed. Moreover, the ethanol flux is far to be predicted by the solution–diffusion model, because no linear trends are observed, even for low values of its driving force. Consequently, despite its simplicity and in contrast to the adsorption–diffusion model, this model does not provide a good approach for the description of mass transfer through zeolite membranes.

Table 4
Parameters fitted in the PV model

Species	Parameter	Adjusted value*
Water	ΔH_{W}^0 [kJ mol^{-1}]	-43 ± 6
	$K_{\mathrm{W}}^{\mathrm{S}}(T_{\mathrm{ref}})$ [Pa^{-1}]	$(1.04 \pm 0.32) \times 10^{-4}$
	$E_{\mathrm{W}}^{\mathrm{S}}$ [kJ mol^{-1}]	35 ± 5
	$D_{\mathrm{W}}^{\mathrm{S}}(0)(T_{\mathrm{ref}})$ [m^2 s^{-1}]	$(2.97 \pm 0.40) \times 10^{-11}$
Ethanol	ΔH_{E}^0 [kJ mol^{-1}]	-37 ± 8
	$K_{\mathrm{E}}^{\mathrm{S}}(T_{\mathrm{ref}})$ [Pa^{-1}]	$(1.17 \pm 0.37) \times 10^{-5}$
	$E_{\mathrm{E}}^{\mathrm{S}}$ [kJ mol ^{1}]	22 ± 6
	$D_{\mathrm{E}}^{\mathrm{S}}(0)(T_{\mathrm{ref}})$ [m^2 s^{-1}]	$(1.17 \pm 0.31) \times 10^{-12}$

* Determined for a confidence interval of 95%.

4.2.4. Discussion

The Maxwell–Stefan approach appears to constitute an excellent basis to account for the PV process of ethanol/water mixtures through inner-side zeolite NaA membranes prepared in our laboratory. A comparison between the fitted values

Table 5
Results of the fits

Species	Sum of squares (SQ) [(kg m^{-2} h^{-1})^2]	Coeffficient correlation (r^2)
Water	6.11×10^{-2}	0.9976
Ethanol	1.06×10^{-4}	0.9886

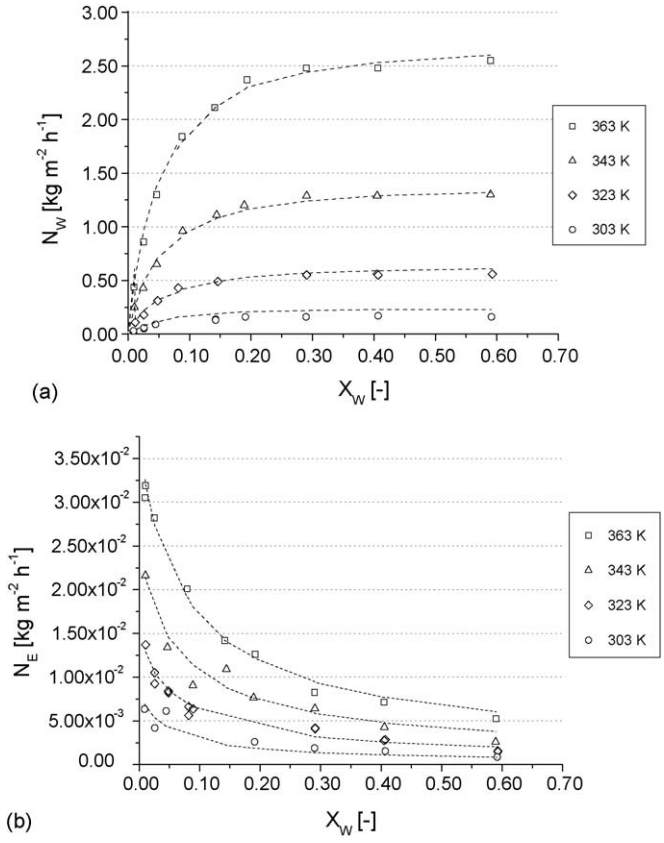

Fig. 7. Evolution of (a) water flux and (b) ethanol flux with feed composition. Dashed lines refer to the fittings to the adsorption–diffusion model. Experimental conditions in Table 2.

obtained for the parameters of the model with literature data is shown in Table 6. Firstly, the computed value for the adsorption enthalpy of water, -43.1 ± 6 kJ mol^{-1}, is of the same order as that found by most of the researchers. Moreover, the adsorption constant for water at T_{ref} (333 K), $(1.04 \pm 0.32) \times 10^{-4}$, is one order of magnitude lower than that reported by Zhu et al. [47] from the unary adsorption isotherm of water on zeolite NaA crystals. The lower value found in this work might be

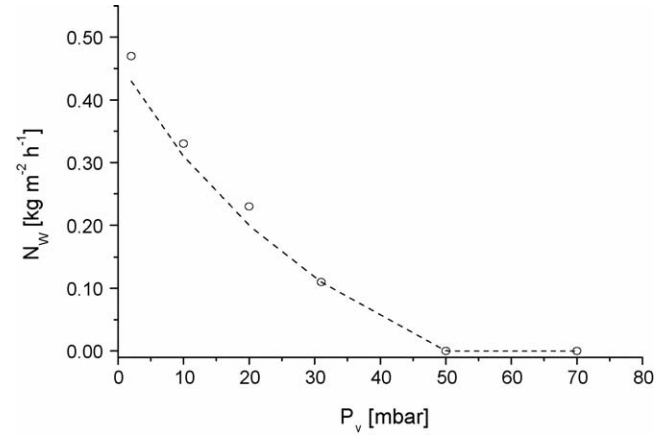

Fig. 8. Evolution of the water flux with the permeate pressure. Experimental conditions: $X_{H_2O} \approx 8.4$–9.0 wt.%; T = 323 K; $P_f = 0.4$ mbar (relative). The dashed line refers to the fitting to the adsorption–diffusion model.

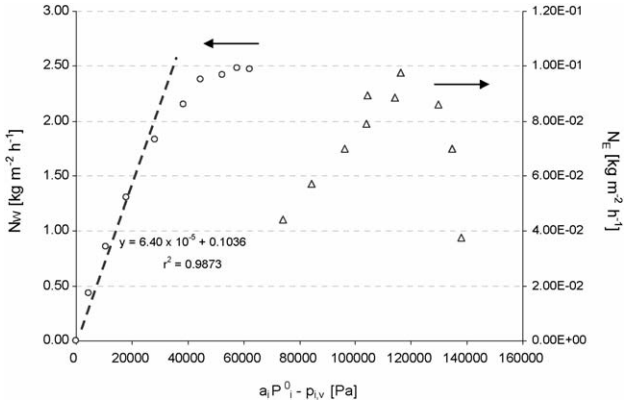

Fig. 9. Trends for water and ethanol fluxes with the driving force $\Delta p_i = a_{i,L} P_i^0 - p_{i,v}$. It can be seen that the solution–diffusion model fails to predict the PV performance of the zeolite NaA prepared.

ascribed to the contribution of non-zeolite pores, which might involve less adsorption strength of water than zeolite pores. In addition, the adsorption constant for water at T_{ref} is one order of magnitude higher than that of ethanol ($(1.04 \pm 0.32) \times 10^{-4}$ Pa^{-1} versus $(1.20 \pm 0.37) \times 10^{-5}$ Pa^{-1}), thus confirming the simplification $\theta_W \gg \theta_E$ made in the derivation of Eqs. (13) and (14). Regarding the values of the activation energy and enthalpy of adsorption for water, the computed value of its effective activation energy is +36 kJ mol^{-1}, which is in fairly good agreement with the value determined from the slopes of the lines in Fig. 4a.

Diffusivity values for both water and ethanol at zero coverage show values of $(2.97 \pm 0.37) \times 10^{-11}$ and $(1.15 \pm 0.29) \times 10^{-12}$ m^2 s^{-1}, respectively (see Table 6). The former is in quite good agreement with the value reported by Shah et al. [16], 3.0–5.0 $\times 10^{-12}$ m^2 s^{-1}, computed from the PV of pure water through a commercial zeolite NaA membrane and by Paoli et al. [48], who found a value $\sim 10^{-9}$–10^{-10} m^2 s^{-1} from their studies by the QENS technique. The diffusivity of ethanol at zero coverage is one order of magnitude lower than that of water. This result is consistent with the differences in the kinetic diameter of both molecules.

Table 6
Energetic and diffusion parameters of water in zeolite NaA

Parameter	Value	References
ΔH_W^S [kJ mol^{-1}]	-61 to -46[a]	[47]
	-56	[46]
	-43	This study
K_W^S [Pa^{-1}]	4.72×10^{-3}[b]	[47]
E_W^S [kJ mol^{-1}]	58	[47]
$D_W^S(0)$ [m^2 s^{-1}]	10^{-9}–10^{-10}[c]	[16]
	3.0–5.0 $\times 10^{-12}$[c]	[48]
	2.97×10^{-11}	This study
$D_E^S(0)$ [m^2 s^{-1}]	1.17×10^{-12}	This study

[a] Isosteric value calculated from DSC from zero coverage to a fully hydrated state.
[b] Determined at 341 K.
[c] Determined at 298–333 K.

On the other hand, although the activation energy for the surface diffusion of ethanol is expected to be much higher than that of water owing to the higher kinetic diameter of the former, the values found from the fittings are quite similar (see Table 6). It should be noted that the activation energy for water found in this study, 35 ± 5 kJ mol^{-1}, is in agreement with the value found by Zhu et al. [47]. However, the activation energy for ethanol, 23 ± 6 kJ mol^{-1}, is much lower than the value that would be expected. This lower value for ethanol activation energy might provide additional evidence of the role intercrystalline diffusion to mass transfer. Since these pores are larger than zeolite windows, the diffusion within them might be less impelled (grain boundaries might behave like fast diffusion paths [49]) and therefore, the activation energy might be reduced.

5. Concluding remarks

The PV performance of zeolite NaA membranes towards the separation of ethanol/water mixtures is strongly dependent on feed composition, temperature and permeate vapor pressure. The adsorption–diffusion model developed in this study under the Maxwell–Stefan approach together with the extended Langmuir equation to describe the adsorption equilibrium in the liquid feed/membrane and vapor permeate/membrane surfaces provides a good basis for the description of the PV process through zeolite NaA membranes. While the water flux is only conjugated to its own driving force, the ethanol flux seems to be conjugated to the former. The adsorption equilibrium at the liquid feed/membrane surface contributes to a greater extent to the PV separation performance. The parameters of the model reflect the contribution of non-zeolite pores to the PV performance of the membrane, together with the dependence of the total flux and selectivity on the feed relative pressure. This study confirms that the solution–diffusion model does not explain the trends observed.

Acknowledgment

The authors gratefully acknowledge the financial support provided by the Spanish Ministry of Education and Science through projects PPQ2000-0467-P4-02 and PPQ2002-04115-C02-02.

References

[1] F. Lipniki, R.W. Field, P.K. Ten, J. Membr. Sci. 153 (1999) 183.
[2] X. Feng, R.Y.M. Huang, Ind. Eng. Chem. Res. 36 (1997) 1048.
[3] Huang, Pervaporation Membrane Separation Processes, Elsevier, Amsterdam, The Netherlands, 1991.
[4] A. Jonquières, R. Clement, P. Lochon, J. Neel, M. Dresch, B. Chretien, J. Membr. Sci. 206 (2002) 87.
[5] H.L. Fleming, Chem. Eng. Prog. (1992) 46.
[6] J.T.F. Keurentjes, G.H.R. Jansen, J.J. Gorissen, Chem. Eng. Sci. 49 (1994) 4681.
[7] J. Coronas, J. Santamaria, Chem. Eng. Sci. 59 (2004) 4879.
[8] C. Casado, A. Urtiaga, D. Gorri, I. Ortiz, Sep. Purif. Technol. 42 (2005) 39.
[9] A.W. Verkerk, P. van Male, M.A.G. Vorstman, J.T.F. Keurentjes, J. Membr. Sci. 193 (2001) 227.
[10] T.C. Bowen, R.D. Noble, J.L. Falconer, J. Membr. Sci. 245 (2004) 1.
[11] M. Pera-Titus, J. Llorens, F. Cunill, R. Mallada, J. Santamaria, Catal. Today 104 (2005) 281.
[12] M.P. Pina, M. Arruebo, M. Felipe, F. Fleta, M.P. Bernal, J. Coronas, M. Menendez, J. Santamaria, J. Membr. Sci. 244 (2004) 141.
[13] X. Xu, Y. Bao, C. Song, W. Yang, J. Liu, L. Lin, J. Membr. Sci. 249 (2005) 51.
[14] T. Gallego-Lizon, E. Edwards, G. Lobiundo, L. Freitas dos Santos, J. Membr. Sci. 197 (2002) 309.
[15] K. Okamoto, H. Kita, K. Horii, K. Tanaka, Ind. Eng. Chem. Res. 40 (2001) 163.
[16] D. Shah, K. Kissick, A. Ghorpade, R. Hannah, D. Bhattacharyya, J. Membr. Sci. 179 (2000) 185.
[17] X. Lin, E. Kikuchi, M. Matsukata, Chem. Commun. (2000) 957.
[18] A. Navajas, R. Mallada, C. Tellez, J. Coronas, M. Menendez, J. Santamaria, Desalination 148 (2002) 25.
[19] S. Li, V.A. Tuan, J.L. Falconer, R.D. Noble, Ind. Eng. Chem. Res. 40 (2001) 1952.
[20] H. Kita, T. Inoue, H. Asamura, K. Tanaka, K. Okamoto, Chem. Commun. (1997) 45.
[21] Y. Morigami, M. Kondo, J. Abe, H. Kita, K. Okamoto, Sep. Purif. Technol. 25 (2001) 251.
[22] H.O.E. Karlsson, G. Trägård, J. Membr. Sci. 76 (1993) 121.
[23] J.G. Wijmans, R.W. Baker, J. Membr. Sci. 107 (1995) 1.
[24] T.C. Bowen, S. Li, R.D. Noble, J.L. Falconer, J. Membr. Sci. 225 (2003) 165.
[25] I. Ortiz, D. Gorri, C. Casado, A. Urtiaga, J. Chem. Technol. Biotechnol. 80 (2005) 397.
[26] M. Nomura, T. Yamaguchi, S. Nakao, J. Membr. Sci. 187 (2001) 203.
[27] M. Pera-Titus, R. Mallada, J. Llorens, F. Cunill, J. Santamaria, J. Membr. Sci. 278 (2006) 401.
[28] R. Krishna, J.A. Wesseling, Chem. Eng. Sci. 48 (1997) 861.
[29] R. Krishna, Chem. Eng. Sci. 45 (1990) 1779.
[30] L.J.P. Van den Broeke, R. Krishna, Chem. Eng. Sci. 50 (1995) 2507.
[31] J.M. van der Graaf, F. Kapteijn, J.A. Moulijn, AIChE J. 45 (1999) 497.
[32] J.M. van der Graaf, F. Kapteijn, J.A. Moulijn, J. Membr. Sci. 144 (1998) 87.
[33] L.J.P. van den Broeke, W.J.W. Bakker, F. Kapteijn, J.A. Moulijn, Chem. Eng. Sci. 54 (1999) 245.
[34] B. Millot, A. Methivier, H. Jobic, H. Moueddeb, J.A. Dalmon, Microporous Mesoporous Mater. 38 (2000) 85.
[35] L.J.P. Van den Broeke, AIChE J. 41 (1995) 2399.
[36] T. Yoshioka, E. Nakanishi, T. Tsuru, M. Asaeda, AIChE J. 47 (2001) 2052.
[37] J. Xiao, J. Wei, Chem. Eng. Sci. 47 (1992) 1123.
[38] A.L. Myers, J.M. Prausnitz, AIChE J. 11 (1965) 121.
[39] E. Costa, J.L. Sotelo, G. Calleja, C. Marrón, AIChE J. 27 (1981) 5.
[40] M. Sakuth, J. Meyer, J. Gmehling, Chem. Eng. Process. 37 (1998) 267.
[41] F. Kapteijn, J.A. Moulijn, R. Krishna, Chem. Eng. Sci. 55 (2000) 2923.
[42] R. Krishna, Int. Commun. Heat Mass Transfer 28 (2001) 337.
[43] D.W. Breck, Zeolite Molecular Sieves-Structure Chemistry and Use, Wiley, New York, 1974.
[44] R. Krishna, R. Baur, Chem. Eng. Sci. 97 (2004) 37.
[45] R.C. Reid, J.M. Prausnitz, B.E. Poling, The Properties of Gases and Liquids, fourth ed., McGraw-Hill, New York, 1987.
[46] J.C.M. Muller, G. Hakvoort, J.C. Jansen, J. Therm. Anal. 53 (1998) 449.
[47] W. Zhu, L. Gora, A.W.C. Van den Berg, F. Kapteijn, J.C. Jansen, J.A. Moulijn, J. Membr. Sci. 253 (2005) 57.
[48] H. Paoli, A. Methivier, H. Jobic, C. Krause, H. Pfeifer, F. Stallmach, J. Kärger, Microporous Mesoporous Mater. 55 (2002) 147.
[49] J. Philibert, Atom movements. Diffusion and Mass Transport in Solids, Les Editions de Physique, 1991.